

## In vivo study of acetylcholine esterase in basal forebrain, amygdala, and cortex in mild to moderate Alzheimer disease

K. Herholz,<sup>a,\*</sup> S. Weisenbach,<sup>a</sup> G. Zündorf,<sup>a</sup> O. Lenz,<sup>a</sup> H. Schröder,<sup>b</sup> B. Bauer,<sup>a</sup>  
E. Kalbe,<sup>a</sup> and W.-D. Heiss<sup>a</sup>

<sup>a</sup>Department of Neurology, University Cologne, and Max-Planck Institute for Neurological Research, Cologne, Germany

<sup>b</sup>Department II of Anatomy—Neuroanatomy, University Cologne, Cologne, Germany

Received 7 April 2003; revised 16 September 2003; accepted 16 September 2003

It is currently unclear whether impairment of the cholinergic system is present in Alzheimer disease (AD) already at an early stage and to what extent it depends on degeneration of the nucleus basalis of Meynert (nbM). We examined acetylcholine esterase activity in vivo in the nbM, the amygdala, and cerebral neocortex. Measurements were performed in normal controls and in patients with mild to moderate AD with positron emission tomography (PET) and C-11-labeled *N*-methyl-4-piperidyl-acetate (MP4A) which is a specific substrate of AChE. AChE activity was reduced significantly in amygdala and cerebral cortex. In contrast, AChE activity and glucose metabolism appeared preserved or even increased in the nbM. The results support the concept that neocortical and amygdaloid functional changes of the cholinergic system are an early and leading event in AD, rather than the consequence of neurodegeneration of basal nuclei.

© 2003 Elsevier Inc. All rights reserved.

**Keywords:** Alzheimer disease; Nucleus basalis Meynert; Acetylcholine esterase; Cerebral glucose metabolism; Positron emission tomography; Amygdala

### Introduction

Evidence for disturbance of cholinergic transmission in Alzheimer disease (AD) was found in many clinical and neuropathological studies (see reviews by Bartus et al., 1982; Coyle et al., 1983). The integrity of the cholinergic system has mostly been studied by histochemistry and immunohistochemistry of its two key enzymes, choline acetyl transferase (ChAT) and acetylcholine esterase (AChE). Cholinergic innervation of cerebral cortex mostly originates from the nucleus basalis of Meynert (nbM) (Mesulam et al., 1983). These neurons and their axons, which stain positive for ChAT and AChE (Mesulam and Geula, 1992), were reduced in autopsy studies of severe AD (Davies and Maloney, 1976; Perry et

al., 1977; Whitehouse et al., 1982) in correlation with dementia severity (Bierer et al., 1995). There is no in vivo tracer for ChAT but nbM cholinergic neurons express ChAT and AChE in a closely related manner (Mesulam and Geula, 1988b). Therefore imaging of AChE is a suitable in vivo indicator to study the integrity of nbM neurons. There is also a substantial reduction of cortical nicotinic binding sites (see review by Wevers and Schröder, 1999). On the other hand, persistence of shrunken cholinergic neurons in nbM in AD was demonstrated (Pearson et al., 1983) and cortical and nbM ChAT activity was found intact in mild AD (Davis et al., 1999; Gilmor et al., 1999; Tiraboschi et al., 2000) or even up-regulated in mild cognitive impairment (Dekosky et al., 2002), challenging the view that loss of cortical cholinergic innervation from nbM is an early and constitutive component of AD.

In recent years, tracers have been developed for in vivo imaging of cerebral AChE with positron emission tomography (PET) (Kilbourn et al., 1996; Namba et al., 1994). We used a piperidine analogue of acetylcholine, C-11-labeled *N*-methyl-4-piperidyl-acetate (MP4A), which enters the brain freely (depending on blood flow) and then accumulates depending on hydrolytic activity of AChE. Reduction of cortical AChE activity in AD has already been described with this technique in previous studies (Herholz et al., 2000; Iyo et al., 1997; Kuhl et al., 1999; Shinotoh et al., 2000). Current clinical PET scanners have reached a spatial resolution of 4 mm (Wienhard et al., 1994) and permit imaging even of small brain nuclei, such as basal forebrain nuclei and the amygdala that exhibit high AChE activity and thus high tracer accumulation. We therefore examined whether there is a reduction of AChE activity in nbM that matches the loss of cortical AChE activity in AD. This should clarify whether loss of cortical AChE activity in AD is due to degeneration of nbM, or whether there is a primarily cortical change of AChE activity that is independent from nbM degeneration (Mufson et al., 1987). As an additional check of local neuronal function, local cerebral glucose metabolism was examined by F-18-2-fluoro-2-deoxy-D-glucose (FDG) PET.

### Patients and methods

Nine patients with probable AD according to NINCDS-ADRDA criteria (3 male, 6 female, age 61.7 ± 7.5 years) were

\* Corresponding author. Neurologische Universitätsklinik und Max-Planck-Institut für neurologische Forschung, Josef-Stelzmann-Str. 9, 50931 Cologne, Germany. Fax: +49-221-4726-298.

E-mail address: karl.herholz@pet.mpin-koeln.mpg.de (K. Herholz).

Available online on ScienceDirect (www.sciencedirect.com.)

included in the study. Patients underwent comprehensive neuropsychological tests for verbal and nonverbal short-term memory, working memory, long-term memory, visuoconstructive ability, speed of information processing, executive functions, and word finding. Dementia severity was determined by the mini-mental status examination (MMSE) (Folstein et al., 1975) that proved mild to moderate dementia (MMSE  $18.9 \pm 4.3$ , range 10–23). Duration of disease was 8–54 months ( $23 \pm 15$ ). All patients had MRI and two PET scans (MP4A and FDG). Patients were compared with age-matched healthy normal volunteers without cognitive complaints and normal neuropsychological test results. Thirteen normal controls (7 male, 6 female, age  $62.5 \pm 8.1$  years) had MP4A PET scans and another group of 12 normal controls (5 male, 7 female, age  $60.9 \pm 3.7$  years) had FDG PET scans. Patients and controls did not use AChE inhibitors or any other drug that could influence central cholinergic activity and gave their written informed consent in accordance with the declaration of Helsinki. The study was approved by the ethics committee of the medical faculty.

For definition of individual macroscopic anatomy, a volume T1-weighted MRI scan on a 1- or 1.5-T scanner and slice thickness 1–2.5 mm was recorded. To assess local AChE activity, 555–740 MBq  $^{11}\text{C}$ -MP4A that were synthesized according to the methods of Irie et al. (1996) with minor modifications as described previously (Herholz et al., 2000) were injected intravenously as a slow bolus.

Cerebral activity was recorded by a PET scanner with 47 slices (ECAT EXACT HR, Siemens-CTI, Knoxville, TN, USA) over 60 min in 3D mode without septa. A dynamic sequence of  $6 \times 30\text{s}$ ,  $2 \times 60\text{s}$ ,  $2 \times 150\text{s}$ , and  $10 \times 300\text{s}$  scans was used. FDG PET scans were acquired in a separate session 20–60 min after intravenous injection of 185–370 MBq FDG. All PET scans were done under standard resting conditions (eyes closed and ears unplugged in a quiet scanner room). A 10-min transmission scan with 3 Ge-68 rods (168 MBq each) was acquired before each scan. ECAT-7 software was used for image reconstruction by filtered backprojection using a ramp filter and including corrections for scatter, attenuation, and decay.

Image processing employed the MPI-Tool (Pietrzyk et al., 1990, 1996), SPM99 (Wellcome Institute of Cognitive Neuroscience, London, U.K.) and VINCI (Max-Planck-Institut für neurologische Forschung, Köln, Germany) software for image registration and reformatting. IDL routines (Research Systems Incorporated, Boulder, CO) were used for placement and evaluation of volumes of interest (VOIs). Processing proceeded with the following steps for each subject. The first 10 MP4A PET scan frames of each series (representing 0–10 min p.i.) were summed. All subsequent frames were coregistered with this early image to adjust for possible head movement during the last 50 min of the scanning session. Then these coregistered last 10 frames (representing 10–60 min p.i.) were

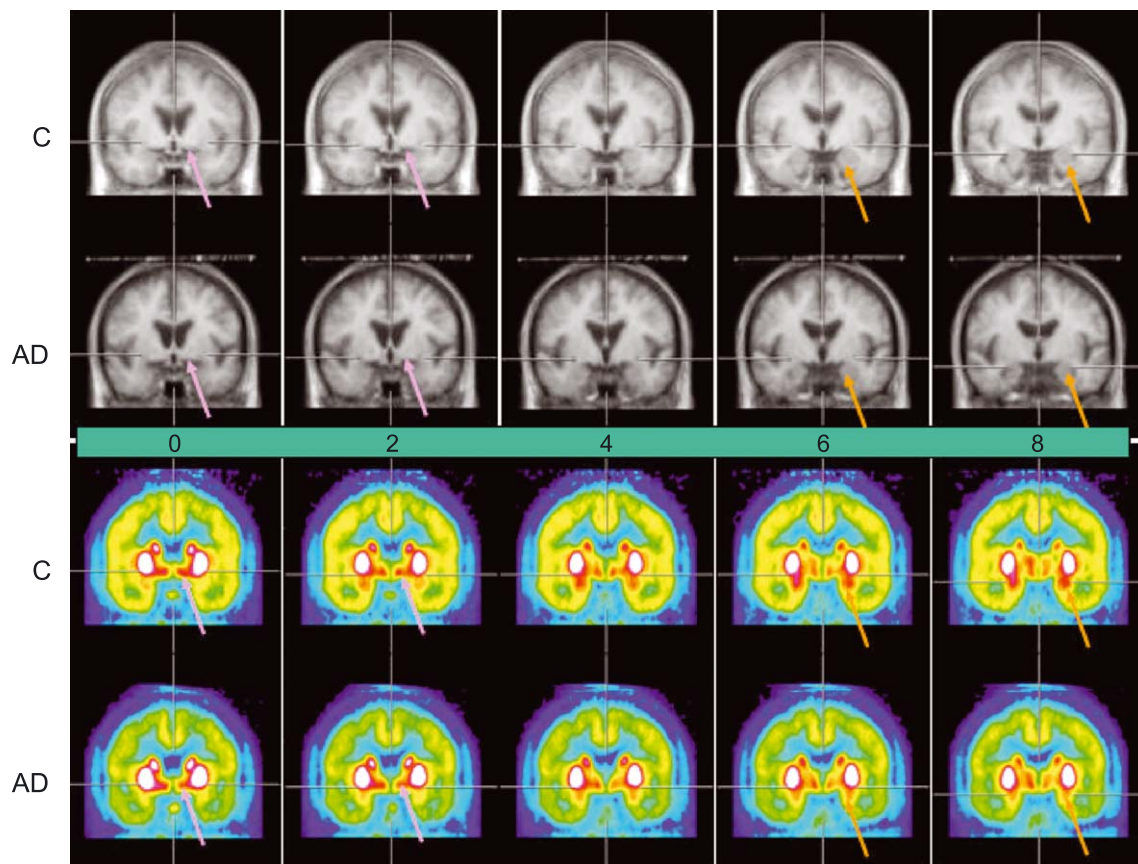


Fig. 1. Average images of controls (C) and AD patients (AD) with stereotactic normalization. Coronal slices (perpendicular to the AC–PC line) are shown, starting at the AC and progressing in 2 mm steps caudally (distance from AC shown in the middle of the figure). MRI images are shown on top, MP4A PET scaled to 65% of maximum brain activity at bottom. The anteromedial and anterolateral parts of the nbM are marked by a pink arrow (the posterior part is located just below the putamen with its very high activity and cannot be separated). The amygdalae are marked by an orange arrow. Please note the progression of the distance between the left and right optic tract from 0 to 8 mm caudal to the AC. This serves as a landmark to compare the anatomical site with the histochemical studies (Hedreen et al., 1984; Mesulam and Geula, 1988b). In AD (bottom row), AChE activity was reduced in cortex and amygdala, but not in nbM.

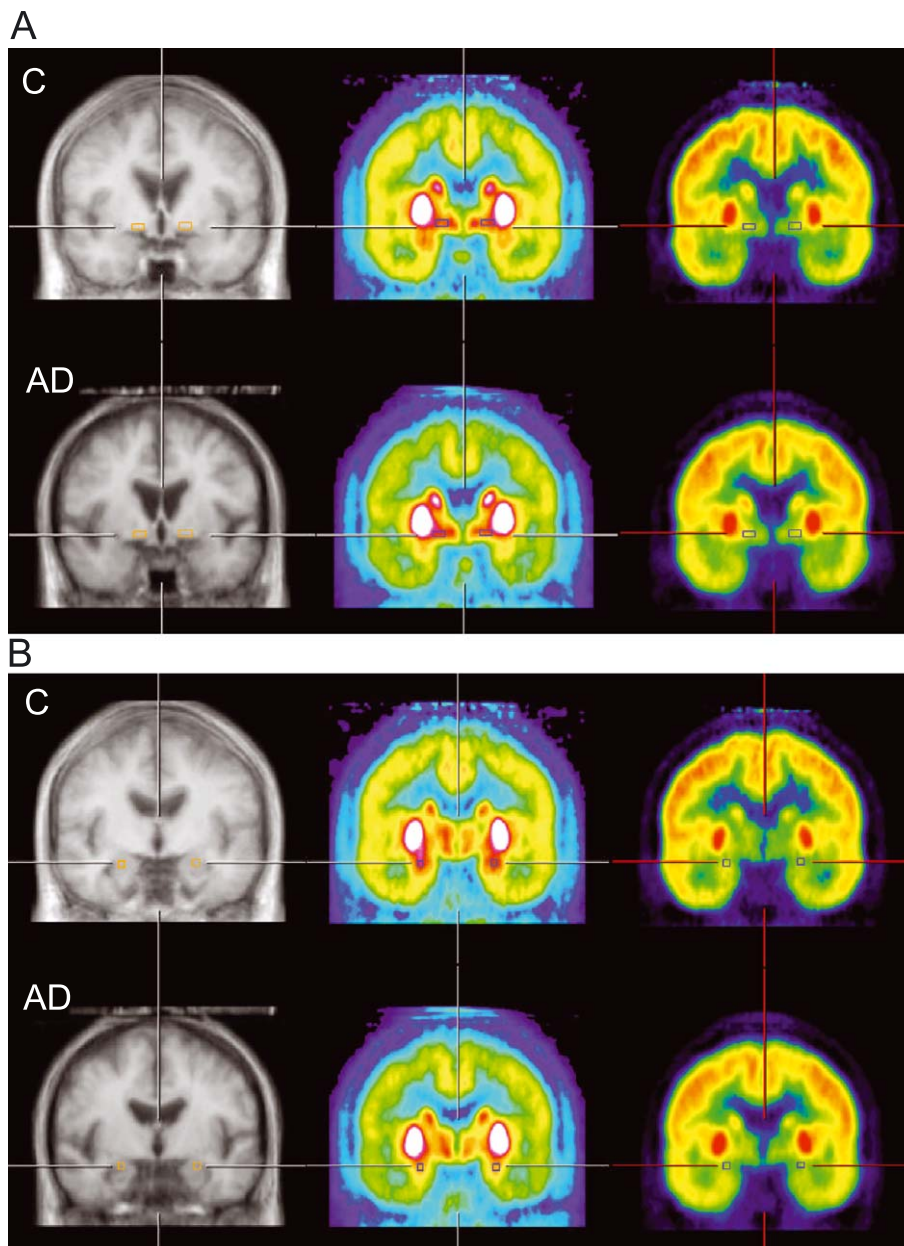


Fig. 2. (A) Normalized average MRI (left column), MP4A PET (middle column, same scaling as in Fig. 1), and FDG PET (right column, scaled to maximum in putamen with 10% background subtraction) of normal controls (top row) and AD patients (bottom row). The coronal slice 2 mm caudally of the anterior commissure with the nbM VOI marked by a box is displayed. Cortical activity (MP4A and FDG) is lower in AD than in controls, but activity in nbM is well preserved. (B) The coronal slice 8 mm caudally of the anterior commissure with the amygdala VOI marked by a box is displayed in the same arrangement as in A. Cortical activity (MP4A and FDG) is lower in AD than in controls. MP4A uptake in amygdala is reduced in AD. FDG uptake in amygdala is relatively low compared to putamen and cortex, and there is no difference between controls and AD.

added, resulting in the MP4A uptake image. The anterior and posterior commissure (AC, PC) were identified on MRI scans, and scans were oriented in transaxial slices in parallel to the AC–PC line. MP4A uptake images and FDG PET scans were coregistered with these MRI scans in standard position. All images were now reformatted to isotropic voxel size of  $1 \times 1 \times 1$  mm by tri-linear interpolation. The anterior, occipital, left, and right lateral poles of each brain were identified on the MRI scans to determine individual brain size for conversion of individual voxel coordinates (all relative to AC) to standard stereotactic coordinates. Some MRI scans did not include the brain vertex in the field of view, thus the conversion

factor for the z-axis was estimated as the average of the conversion factors in the x and y direction. VOI were boxes of fixed size and were placed according to stereotactic coordinates (Talairach and Tournoux, 1988) with individual adjustment to anatomical landmarks on MRI or local maxima of AChE activity, as explained in detail below.

The VOIs to gauge the nbM were placed as identified in histochemical studies (Hedreen et al., 1984; Mesulam and Geula, 1988b) and in MRI studies (Sasaki et al., 1995) with reference to anatomical landmarks (anterior commissure, 3rd ventricle, optic tract) that are visible on MRI (see Fig. 1). The size of this VOI, a  $7 \times$

Table 1  
Stereotactic coordinates of VOI centers (mm, relative to anterior commissure)

VOI	x		y		z	
	Mean	SD	Mean	SD	Mean	SD
<i>Amygdala L</i>						
AD	-24.1	1.3	-7.0	2.2	-11.9	0.3
C	-22.7	2.0	-8.7	1.6	-11.8	0.7
<i>Amygdala R</i>						
AD	23.7	2.8	-7.4	2.3	-12.0	0.0
C	22.8	1.7	-7.7	1.7	-12.3	1.1
<i>nbM L</i>						
AD	-12.8	0.7	-2.0	0.0	-4.1	0.3
C	-12.5	0.5	-2.0	0.0	-4.7	0.5
<i>nbM R</i>						
AD	13.0	0.7	-2.0	0.0	-4.0	0.5
C	12.8	0.7	-2.0	0.0	-4.2	0.9
<i>Occipital L</i>						
AD	-40.3	1.7	-78.3	3.3	0.0	0.0
C	-40.4	4.3	-79.1	2.8	0.0	0.0
<i>Occipital R</i>						
AD	38.1	2.5	-78.9	2.1	0.0	0.0
C	38.9	3.0	-78.3	3.3	0.0	0.0
<i>Putamen L</i>						
AD	-25.4	1.7	-2.1	0.1	5.1	0.3
C	-26.2	1.3	-2.0	0.1	5.5	1.1
<i>Putamen R</i>						
AD	26.3	1.6	-2.1	0.1	4.1	1.3
C	26.6	1.8	-2.0	0.1	5.5	1.4

C: controls.

3 × 3 mm box, was adapted to the extent of nbM, as depicted in Fig. 3A of (Mesulam and Geula, 1988b). On each subject's MRI, it was placed within the substantia innominata in a coronal slice 2 mm caudal to the interhemispheric crossing of the anterior commissure (corresponding to Fig. 10F of Hedreen et al., 1984) at the floor of the forebrain just above and lateral to the optic tract (Fig. 2A). Its location was ventral to the anterior commissure, which separates the substantia innominata from the pallidum.

The putamen VOIs (3 × 3 × 3 mm) were placed at stereotactic coordinates -26, -2, 5 (left) and 26, -2, 5 (right) with adjustment of up to 3 mm along the x and z axis to place the VOI in maximum

AChE activity (Fig. 2B). Amygdala VOIs were placed at -23, -8, -12 (left) and 23, -8, -12 (right) with adjustment mainly within the x-y plane to capture local maximum AChE activity. Occipital VOIs were placed in the lateral occipital cortex at -40, -78, 0 (left) and 40, -78, 0 (right) with adjustment within the x-y plane to sample convexity cortex and to avoid sulci. Mean coordinates of VOI centers are shown in Table 1.

Mean MP4A and FDG uptake values were determined for each VOI. They were normalized to uptake in putamen (average of left and right). To check kinetic curves, VOIs were re-transferred into the original realigned MP4A frame series.

In addition, we studied the cortical distribution of AChE activity by calculating  $k_3$  values for each voxel in standard stereotactic space (without reference to individual MRIs) according to a previously described procedure that uses the putamen curve as a reference and involves image smoothing with a 10-mm Gaussian filter (Herholz et al., 2001; Zündorf et al., 2002). By use of a VOI mask representing frontal, parietal, temporal, and occipital lobes, we determined mean  $k_3$  values for these structures in each individual and compared them between AD and controls.

Analysis of variance was used to compare values between AD and controls. The SAS software package (SAS, Cary, NC) was used for statistical calculations.

## Results

### MP4A uptake and glucose metabolism in nbM, amygdala, and cortex

On visual inspection of MP4A images that were recorded 10–60 min after i.v. injection, higher AChE activity than in surrounding tissue was visible in all subjects in the area of the nbM and the amygdala (Fig. 1), permitting unambiguous placement of VOIs in the antero-mesial and antero-lateral parts of the nbM, in the amygdala, and in occipital cortex according to the rules described in the Patients and methods section. Stereotactic coordinates of VOI centers (Table 1) showed very little variation in the nbM (SD less than 1 mm), consistent with its location very close to AC as the anchor point of the coordinate system. Variation was slightly larger in the amygdala, and relatively largest (with a SD of still less than 4 mm) in the occipital cortex, which is known as an area of relatively large anatomical variability in the brain. There was mild enlargement of the 3rd ventricle and clearly evident atrophy in the temporal lobe in AD, but this did not result in significant differences of VOI locations between controls and AD.

Table 2  
MP4A uptake (relative to putamen)

Region	Side	MP4A uptake (mean ± SD)		FDG uptake (mean ± SD)	
		Controls	AD	Controls	AD
Nucleus basalis of Meynert (nbM)	left	0.50 ± 0.07	0.51 ± 0.08	0.47 ± 0.05	0.53 ± 0.05**
	right	0.50 ± 0.07	0.56 ± 0.04**	0.51 ± 0.03	0.54 ± 0.06
Amygdala	left	0.59 ± 0.05	0.51 ± 0.06*	0.55 ± 0.05	0.56 ± 0.09
	right	0.60 ± 0.05	0.54 ± 0.07*	0.59 ± 0.05	0.57 ± 0.07
Occipital cortex	left	0.32 ± 0.03	0.26 ± 0.06*	0.74 ± 0.07	0.64 ± 0.09*
	right	0.33 ± 0.04	0.24 ± 0.08*	0.75 ± 0.08	0.63 ± 0.15*

\* Significantly decreased in AD ( $P < 0.05$ ,  $t$  test).

\*\* Significantly increased in AD ( $P < 0.05$ ,  $t$  test).

Table 3  
Cortical AChE activity (MP4A  $k_3$ ,  $\text{min}^{-1}$ , mean  $\pm$  SD)

Lobe	Controls	AD	Significance ( $P$ )
Frontal	0.0978 $\pm$ 0.0088	0.0803 $\pm$ 0.0121	0.0008
Temporal	0.1007 $\pm$ 0.0099	0.0688 $\pm$ 0.0064	<0.0001
Parietal	0.0881 $\pm$ 0.0108	0.0620 $\pm$ 0.0073	<0.0001
Occipital	0.0861 $\pm$ 0.0088	0.0597 $\pm$ 0.0067	<0.0001

In AD, MP4A uptake was significantly reduced in amygdala by 12% ( $P = 0.004$  on left side,  $P = 0.03$  on right side) and in occipital cortex by 23% ( $P = 0.02$  left,  $P = 0.01$  right). In contrast, there was no reduction of MP4A uptake in nbM (Table 2). On the right side, there was even an increase of nbM MP4A uptake by 12% ( $P = 0.03$ ). FDG uptake was reduced in occipital cortex ( $P = 0.008$  left,  $P = 0.03$  right) and was unchanged in amygdala. In nbM, there was a tendency toward higher FDG uptake in patients than in normals by 13% ( $P = 0.01$ ) on the left side and by 6% ( $P = 0.09$ ) on the right side.

#### Analysis of MP4A kinetics

Kinetic tracer uptake curves of amygdala and nbM became parallel to putamen 10 min after injection, resulting in region to reference ratios (Fig. 2) that were constant (apart from stochastic fluctuations). In nbM, the early parts of the curves were so noisy that it was not possible to apply curve fits for determination of  $k_3$  and, therefore, the analysis of nbM data in this study was limited to 10–60 min uptake values, as reported above. In amygdala, the early parts were somewhat less noisy and showed a very rapid decline, consistent with high  $k_3$  values in the order of  $0.4 \text{ min}^{-1}$ . Only in cortex a well-defined decline of activity (relative to the reference region) was observed that allowed reliable  $k_3$  calculation by curve fitting (Herholz et al., 2001; Zündorf et al., 2002).

Cortical  $k_3$  values were reduced significantly in all lobes (Table 3). The effect was largest in temporal (reduction by 33.7%), occipital (30.7%), and parietal (29.6%) (all  $P < 0.0001$ ), whereas the frontal lobe showed the least, but still highly significant reduction by 17.9% ( $P = 0.0008$ ).

#### Discussion

Neither PET nor MRI can provide the anatomical resolution that would be needed to identify nbM on the scans in a way that is as accurate as histochemistry. Yet, guidance by macroscopic landmarks (mainly anterior commissure, 3rd ventricle, and optical tract) visible on MRI permits placement of VOIs to sample nbM activity. Histochemical studies of the basal forebrain have shown that AChE-positive neurons are located in the nbM, which comprises the largest number, and in the diagonal band of Broca (dbB) and the medial septum (Hedreen et al., 1984). The nbM has its largest extension along the  $x$  axis and is located in the substantia innominata ventral of the anterior commissure and the pallidum. The location of our VOI could be compared very closely on coronal sections with anatomical studies in humans (Hedreen et al., 1984; Mesulam and Geula, 1988b) by using the optic tract as a landmark, which moves from a medial to a more lateral position as slices progress from rostral to

caudal. It was centered just 2 mm caudally to the anterior commissure (see Fig. 1). In this coronal plane, the optic tract just leaves the chiasma and the nbM is located dorsal and lateral of the optic tract. At this location, our VOI mainly comprises the anteromedial and anterolateral subsectors, which project to cingulate, frontal, and parietal cortex and to the amygdala (Mesulam and Geula, 1988b). The diagonal band of Broca is located somewhat more rostrally and ventrally and therefore is not likely to be included in our VOI. AChE-positive hypothalamic nuclei are mostly located more caudally (approximately 8 mm from the AC plane) adjacent to the 3rd ventricle, outside of the VOI. Yet, since there are no macroscopically visible borders between these different AChE-positive structures, we cannot exclude minor contamination of AChE activity in the nbM VOI from non-nbM structures.

Another issue in quantitation of nbM AChE activity is its position relatively close to the putamen with very high AChE activity and the limits of PET spatial resolution. The distance between our VOI, sampling mainly the anteromedial and anterolateral part of the nbM, and the putamen center was 16 mm. The nearest distance to the ventral part of the putamen was 8 mm, which is twice the scanner resolution (FWHM) at which only approximately 1/10 of putamen activity is expected as spillover into the nbM VOI. Spillover is the same in controls and AD, and we therefore can rule out a relevant bias in the measurement of nbM MP4A uptake. Unfortunately, the close proximity between the posterior part of nbM, which is believed to project mainly to temporal cortex (Mesulam and Geula, 1988b), did not permit to place the VOI in a way to include that part of the nbM without risking major contamination from putaminal activity, and we therefore preferred to exclude it.

Due to the small size of the nbM which is in the order of the resolution of our PET scanner in the  $z$  direction, we expect some underestimation of AChE activity due to incomplete recovery of counts (Hoffman et al., 1979). We simulated partial volume effects by construction of a digital template of the relevant anatomical structures with homogenous AChE activity based on the actual distribution of measured activity in a normal subject. High activity in the striatum was set to 100 units, intermediate activity in pallidum and other basal forebrain structures outside of the nbM VOI was set to 50, other brain tissue to 10, and CSF to 0. That template was then filtered with a 3D Gaussian kernel of 6 mm width, corresponding to the scanner resolution, and resulting activity in the nbM VOI was analyzed. We simulated a reduction of 20% (from 50 to 40 units) in the nbM VOI and found that the apparent reduction of nbM activity in the filtered data was still 15% if adjacent regions did not change their activity. Thus, a decline of nbM MP4A uptake in the same order as in the most affected cortical region (by 23% in occipital cortex) would not have remained undetected with our method.

Due to the small size of the nbM VOI, dynamic uptake curves (Fig. 3) display a high level of noise in the early parts of the curve that obviates dynamic curve fitting and calculation of valid  $k_3$  values. Therefore, analysis was restricted to cumulative uptake values 10–60 min after i.v. injection, which represent the combined effects of blood flow and AChE activity (Herholz et al., 2001; Koeppe et al., 1999). Any loss of cholinergic neurons in nbM would lead to local loss of expression of AChE, which is required for MP4A trapping. Furthermore, neurodegeneration generally leads to reduction of local blood flow and glucose metabolism (Kuhl, 1984). Thus, with the preservation of both

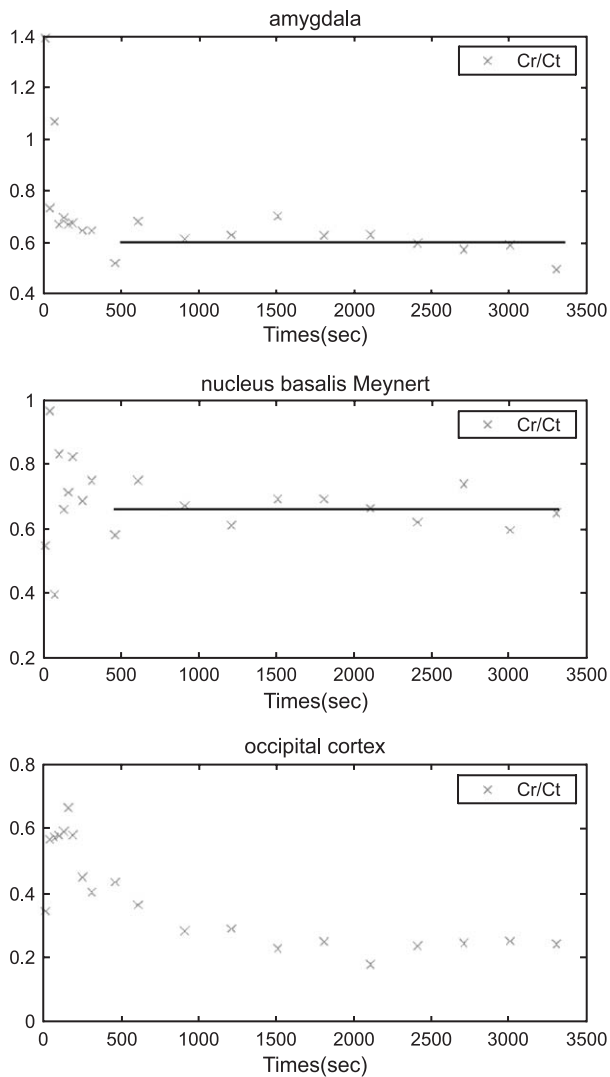


Fig. 3. Kinetic tracer uptake curves (VOI counts relative to reference counts in putamen) of an AD patient. A typical decline up to 1500 s (25 min), due to lower AChE than in the reference region, is seen in occipital cortex. The nbM and amygdala have high AChE activity similar to the reference region, resulting in a horizontal line (with stochastic fluctuations) from 10 to 60 min.

tracers, MP4A and FDG, we did not find any evidence of nbM degeneration.

Our amygdala VOI was centered in the coronal plane 8 mm caudally to the anterior commissure. Anatomical and histochemical studies of amygdala subdivisions (Aggleton, 2000; Vereecken, 1993) indicate that the basal nuclei which show the most intense AChE staining (Brashear et al., 1988; Sims and Williams, 1990; Svendsen and Bird, 1985) are well represented in this slice. These basal amygdaloid nuclei have reciprocal projections to the nbM complex, thalamus, hypothalamus, and hippocampus (Chow and Cummings, 2000; Vereecken, 1993). The lateral amygdaloid nucleus which has more reciprocal connections to neocortical areas and does not show AChE staining is located more rostrally and laterally and therefore not included in our VOI.

AD patients showed a clear enlargement of the lateral horn of the temporal ventricle and atrophy of the amygdala, consistent

with previous MRI studies (see Wahlund, 1996 for review). Severe atrophy of the magnocellular regions of the amygdala with reciprocal projections to nbM has been reported in AD (Scott et al., 1991). Thus, we cannot exclude that the apparent reduction of MP4A uptake may at least partially be due to partial volume effects and incomplete quantitative recovery of activity that requires further study including quantitative correction for atrophy. Yet, the absence of reduced FDG uptake argues against the assumption that the reduction of MP4A uptake was merely due to atrophy. Reduced AChE activity in amygdala is consistent not only with previous PET results (Shinotoh et al., 2000), but also with a reduced amygdaloid ChAT activity in AD (Rossor et al., 1982).

Preservation of nbM is in contrast with a significant decline of AChE activity in cortex and amygdala. This suggests that AChE is already disappearing from the terminals of cholinergic neurons in cortex before there is a reduction of AChE signal at the cell bodies in nbM. This is consistent with reports that degeneration of the nbM, as reported in severe AD, is the consequence of retrograde degeneration (“dying back”) following functional impairment of cortical axons (Candy et al., 1983; Sofroniew et al., 1983; Wevers et al., 1999). A minor contribution of cortical AChE activity probably stems from cortical cholinergic neurons and dendrites, which also degenerate in AD (Mesulam and Geula, 1988a). The degeneration of cholinergic axons in cortical association areas could possibly be due to deposition of neurotoxic beta amyloid in association neocortex very early in AD (Thal et al., 2002).

Specific markers for cholinergic receptors and transporters in cortex could provide further clarification of the cholinergic changes in AD. Recent studies indicate a reduction of nicotinic receptors (Nordberg, 2001; Perry et al., 2000; Wevers et al., 1999), a change in muscarinic receptor subtypes (Flynn et al., 1995), and a reduction of choline and acetylcholine transporters (Sihver et al., 1999). Yet, it is not clear whether these changes are present already at early stages of the disease. In a SPECT study with I-123-iodobenzovesamicol, only a small reduction of cholinergic nerve terminals was found in mild AD, mainly in temporal cortex and hippocampus and only in patients with early onset AD (Kuhl et al., 1996). C-11-nicotine PET has been used to demonstrate a reduction of cortical nicotinic receptors in vivo (Nordberg et al., 1995) but its potential is limited by high unspecific binding. PET tracers to overcome these limitations are currently being developed (Chefer et al., 2003; Mulholland et al., 1998; Podruchny et al., 2003; Sihver et al., 2000; Zubieta et al., 2001).

The reduction of AChE in all cortical areas is consistent with most post-mortem data (Beach et al., 1997; Bierer et al., 1995; Perry et al., 1991) and with previous PET studies (Herholz et al., 2001; Kuhl et al., 1999; Shinotoh et al., 2000). The noninvasive procedure used for  $k_3$  quantification in the present study has been validated by the more invasive procedure with arterial blood sampling (Herholz et al., 2001). Quantitation of  $k_3$  depends on the slope of the uptake curve but not on its absolute scale. It is therefore not sensitive to partial volume effects due to atrophy which would affect all kinetic data points to the same degree. Thus, the observed decrease of cortical AChE activity is not possibly an artifact that could be caused by atrophy.

In conclusion, our study lends further support to the concept that neocortical and amygdaloid functional changes of the cholinergic system are an early and leading event in AD, rather than the consequence of neurodegeneration of basal nuclei.

## Acknowledgments

The authors thank Prof. Lackner and Dr. von Smekal for providing the MRI scans. Part of the study was supported by the Deutsche Forschungsgemeinschaft (HE 2664/3).

## References

- Aggleton, J.P., 2000. *The Amygdala*. Oxford Univ. Press, Oxford, UK.
- Bartus, R.T., Dean, R.L., Beer, B., Lippa, A.S., 1982. The cholinergic hypothesis of geriatric memory dysfunction. *Science* 217, 408–414.
- Beach, T.G., Honer, W.G., Hughes, L.H., 1997. Cholinergic fibre loss associated with diffuse plaques in the non-demented elderly: the pre-clinical stage of Alzheimer's disease? *Acta Neuropathol. (Berl.)* 93, 146–153.
- Bierer, L.M., Haroutunian, V., Gabriel, S., Knott, P.J., Carlin, L.S., Purohit, D.P., Perl, D.P., Schmeidler, J., Kanof, P., Davis, K.L., 1995. Neurochemical correlates of dementia severity in Alzheimer's disease: relative importance of the cholinergic deficits. *J. Neurochem.* 64, 749–760.
- Brashear, H.R., Godec, M.S., Carlsen, J., 1988. The distribution of neuritic plaques and acetylcholinesterase staining in the amygdala in Alzheimer's disease. *Neurology* 38, 1694–1699.
- Candy, J.M., Perry, R.H., Perry, E.K., Irving, D., Blessed, G., Fairbairn, A.F., Tomlinson, B.E., 1983. Pathological changes in the nucleus basalis of Meynert in Alzheimer's and Parkinson's disease. *J. Neurol. Sci.* 59, 277–289.
- Chefer, S.I., London, E.D., Koren, A.O., Pavlova, O.A., Kurian, V., Kimes, A.S., Horti, A.G., Mukhin, A.G., 2003. Graphical analysis of 2-[18F]FA binding to nicotinic acetylcholine receptors in rhesus monkey brain. *Synapse* 48, 25–34.
- Chow, T.W., Cummings, J.L., 2000. The amygdala and Alzheimer's disease. In: Aggleton, J.P. (Ed.), *The Amygdala*. Oxford Univ. Press, Oxford, UK, pp. 655–680.
- Coyle, J.T., Price, D.L., Delong, M.R., 1983. Alzheimer's disease: a disorder of cortical cholinergic innervation. *Science* 219, 1184–1190.
- Davies, P., Maloney, A.J., 1976. Selective loss of central cholinergic neurons in Alzheimer's disease. *Lancet* 2, 1403.
- Davis, K.L., Mohs, R.C., Marin, D., Purohit, D.P., Perl, D.P., Lantz, M., Austin, G., Haroutunian, V., 1999. Cholinergic markers in elderly patients with early signs of Alzheimer disease. *JAMA* 281, 1401–1406.
- Dekosky, S.T., Ikonomic, M.D., Styren, S.D., Beckett, L., Wisniewski, S., Bennett, D.A., Cochran, E.J., Kordower, J.H., Mufson, E.J., 2002. Upregulation of choline acetyltransferase activity in hippocampus and frontal cortex of elderly subjects with mild cognitive impairment. *Ann. Neurol.* 51, 145–155.
- Flynn, D.D., Ferrari-DiLeo, G., Mash, D.C., Levey, A.I., 1995. Differential regulation of molecular subtypes of muscarinic receptors in Alzheimer's disease. *J. Neurochem.* 64, 1888–1891.
- Folstein, M.F., Folstein, S.E., McHugh, P.R., 1975. "Mini-mental state". A practical method for grading the cognitive state of patients for the clinician. *J. Psychiatr. Res.* 12, 189–198.
- Gilmore, M.L., Erickson, J.D., Varoqui, H., Hersh, L.B., Bennett, D.A., Cochran, E.J., Mufson, E.J., Levey, A.I., 1999. Preservation of nucleus basalis neurons containing choline acetyltransferase and the vesicular acetylcholine transporter in the elderly with mild cognitive impairment and early Alzheimer's disease. *J. Comp. Neurol.* 411, 693–704.
- Hedreen, J.C., Struble, R.G., Whitehouse, P.J., Price, D.L., 1984. Topography of the magnocellular basal forebrain system in human brain. *J. Neuropathol. Exp. Neurol.* 43, 1–21.
- Herholz, K., Bauer, B., Wienhard, K., Kracht, L., Mielke, R., Lenz, O., Strotmann, T., Heiss, W.-D., 2000. In-vivo measurements of regional acetylcholine esterase activity in degenerative dementia: comparison with blood flow and glucose metabolism. *J. Neural Transm.* 12, 1457–1468.
- Herholz, K., Lercher, M., Wienhard, K., Bauer, B., Lenz, O., Heiss, W.-D., 2001. PET measurement of cerebral acetylcholine esterase activity without blood sampling. *Eur. J. Nucl. Med.* 28, 472–477.
- Hoffman, E.J., Huang, S.C., Phelps, M.E., 1979. Quantitation in positron emission computed tomography: 1. Effect of object size. *J. Comput. Assist. Tomogr.* 3, 299–308.
- Irie, T., Fukushi, K., Namba, H., Iyo, M., Tamagami, H., Nagatsuka, S., Ikota, N., 1996. Brain acetylcholinesterase activity—Validation of a PET tracer in a rat model of Alzheimer's disease. *J. Nucl. Med.* 37, 649–655.
- Iyo, M., Namba, H., Fukushi, K., Shinotoh, H., Nagatsuka, S., Sahara, T., Sudo, Y., Uzuki, K., Rie, T., 1997. Measurement of acetylcholinesterase by positron emission tomography in the brains of healthy controls and patients with Alzheimer's disease. *Lancet* 349, 1805–1809.
- Kilbourn, M.R., Snyder, S.E., Sherman, P.S., Kuhl, D.E., 1996. In vivo studies of acetylcholinesterase activity using a labeled substrate, *n*-[C-11]methylpiperidin-4-yl propionate ([C-11]PMP). *Synapse* 22, 123–131.
- Koeppel, R.A., Frey, K.A., Snyder, S.E., Meyer, P., Kilbourn, M.R., Kuhl, D.E., 1999. Kinetic modeling of *N*-[11C]methylpiperidin-4-yl propionate: alternatives for analysis of an irreversible positron emission tomography trace for measurement of acetylcholinesterase activity in human brain. *J. Cereb. Blood Flow Metab.* 19, 1150–1163.
- Kuhl, D.E., 1984. Imaging local brain function with emission computed tomography. *Radiology* 150, 625–631.
- Kuhl, D.E., Minoshima, S., Fessler, J.A., Frey, K.A., Foster, N.L., Ficaro, E.P., Wieland, D.M., Koeppel, R.A., 1996. In vivo mapping of cholinergic terminals in normal aging, Alzheimer's disease, and Parkinson's disease. *Ann. Neurol.* 40, 399–410.
- Kuhl, D.E., Koeppel, R.A., Minoshima, S., Snyder, S.E., Ficaro, E.P., Foster, N.L., Frey, K.A., Kilbourn, M.R., 1999. In vivo mapping of cerebral acetylcholinesterase activity in aging and Alzheimer's disease. *Neurology* 52, 691–699.
- Mesulam, M.M., Geula, C., 1988a. Acetylcholinesterase-rich pyramidal neurons in the human neocortex and hippocampus: absence at birth, development during the life span, and dissolution in Alzheimer's disease. *Ann. Neurol.* 24, 765–773.
- Mesulam, M.M., Geula, C., 1988b. Nucleus basalis (Ch4) and cortical cholinergic innervation in the human brain: observations based on the distribution of acetylcholinesterase and choline acetyltransferase. *J. Comp. Neurol.* 275, 216–240.
- Mesulam, M.M., Geula, C., 1992. Overlap between acetylcholinesterase-rich and choline acetyltransferase-positive (cholinergic) axons in human cerebral cortex. *Brain Res.* 577, 112–120.
- Mesulam, M.M., Mufson, E.J., Levey, A.I., Wainer, B.H., 1983. Cholinergic innervation of cortex by the basal forebrain: cytochemistry and cortical connections of the septal area, diagonal band nuclei, nucleus basalis (substantia innominata), and hypothalamus in the rhesus monkey. *J. Comp. Neurol.* 214, 170–197.
- Mufson, E.J., Kehr, A.D., Wainer, B.H., Mesulam, M.M., 1987. Cortical effects of neurotoxic damage to the nucleus basalis in rats: persistent loss of extrinsic cholinergic input and lack of transsynaptic effect upon the number of somatostatin-containing, cholinesterase-positive, and cholinergic cortical neurons. *Brain Res.* 417, 385–388.
- Mulholland, G.K., Wieland, D.M., Kilbourn, M.R., Frey, K.A., Sherman, P.S., Carey, J.E., Kuhl, D.E., 1998. [18F]fluoroethoxy-benzovesamicol, a PET radiotracer for the vesicular acetylcholine transporter and cholinergic synapses. *Synapse* 30, 263–274.
- Namba, H., Irie, T., Fukushi, K., Iyo, M., 1994. In vivo measurement of acetylcholinesterase activity in the brain with a radioactive acetylcholine analog. *Brain Res.* 667, 278–282.
- Nordberg, A., 2001. Nicotinic receptor abnormalities of Alzheimer's disease: therapeutic implications. *Biol. Psychiatry* 49, 200–210.
- Nordberg, A., Lundqvist, H., Hartvig, P., Lilja, A., Langstrom, B., 1995. Kinetic analysis of regional (S)(-)-11C-nicotine binding in normal and Alzheimer brains—in vivo assessment using positron emission tomography. *Alzheimer Dis. Assoc. Disord.* 9, 21–27.

- Pearson, R.C., Sofroniew, M.V., Cuello, A.C., Powell, T.P., Eckenstein, F., Esiri, M.M., Wilcock, G.K., 1983. Persistence of cholinergic neurons in the basal nucleus in a brain with senile dementia of the Alzheimer's type demonstrated by immunohistochemical staining for choline acetyltransferase. *Brain Res.* 289, 375–379.
- Perry, E.K., Perry, R.H., Blessed, G., Tomlinson, B.E., 1977. Necropsy evidence of central cholinergic deficits in senile dementia. *Lancet* 1, 189.
- Perry, E.K., McKeith, I., Thompson, P., Marshall, E., Kerwin, J., Jabeen, S., Edwardson, J.A., Ince, P., Blessed, G., Irving, D., 1991. Topography, extent, and clinical relevance of neurochemical deficits in dementia of Lewy body type Parkinson's disease, and Alzheimer's disease. *Ann. N.Y. Acad. Sci.* 640, 197–202.
- Perry, E., Martin-Ruiz, C., Lee, M., Griffiths, M., Johnson, M., Piggott, M., Haroutunian, V., Buxbaum, J.D., Nasland, J., Davis, K., Gotti, C., Clementi, F., Tzartos, S., Cohen, O., Soreq, H., Jaros, E., Perry, R., Ballard, C., McKeith, I., Court, J., 2000. Nicotinic receptor subtypes in human brain ageing Alzheimer and Lewy body diseases. *Eur. J. Pharmacol.* 393, 215–222.
- Pietrzyk, U., Herholz, K., Heiss, W.D., 1990. Three-dimensional alignment of functional and morphological tomograms. *J. Comput. Assist. Tomogr.* 14, 51–59.
- Pietrzyk, U., Herholz, K., Schuster, A., von Stockhausen, H.M., Lucht, H., Heiss, W.D., 1996. Clinical applications of registration and fusion of multimodality brain images from PET, SPECT, CT, and MRI. *Eur. J. Radiol.* 21, 174–182.
- Podruchny, T.A., Connolly, C., Bokde, A., Herscovitch, P., Eckelman, W.C., Kiesewetter, D.O., Sunderland, T., Carson, R.E., Cohen, R.M., 2003. In vivo muscarinic 2 receptor imaging in cognitively normal young and older volunteers. *Synapse* 48, 39–44.
- Rossor, M.N., Svendsen, C., Hunt, S.P., Mountjoy, C.Q., Roth, M., Iversen, L.L., 1982. The substantia innominata in Alzheimer's disease: an histochemical and biochemical study of cholinergic marker enzymes. *Neurosci. Lett.* 28, 217–222.
- Sasaki, M., Ehara, S., Tamakawa, Y., Takahashi, S., Tohgi, H., Sakai, A., Mita, T., 1995. MR anatomy of the substantia innominata and findings in Alzheimer disease: a preliminary report. *AJNR Am. J. Neuroradiol.* 16, 2001.
- Scott, S.A., Dekosky, S.T., Scheff, S.W., 1991. Volumetric atrophy of the amygdala in Alzheimer's disease: quantitative serial reconstruction. *Neurology* 41, 351–356.
- Shinotoh, H., Namba, H., Fukushi, K., Nagatsuka, S., Tanaka, N., Aotsuka, A., Ota, T., Tanada, S., Irie, T., 2000. Progressive loss of cortical acetylcholinesterase activity in association with cognitive decline in Alzheimer's disease: a positron emission tomography study. *Ann. Neurol.* 48, 194–200.
- Sihver, W., Gillberg, P.G., Svensson, A.L., Nordberg, A., 1999. Autoradiographic comparison of [<sup>3</sup>H](–)nicotine, [<sup>3</sup>H]cytisine and [<sup>3</sup>H]epibatidine binding in relation to vesicular acetylcholine transport sites in the temporal cortex in Alzheimer's disease. *Neuroscience* 94, 685–696.
- Sihver, W., Langstrom, B., Nordberg, A., 2000. Ligands for in vivo imaging of nicotinic receptor subtypes in Alzheimer brain. *Acta Neurol. Scand., Suppl.* 176, 27–33.
- Sims, K.S., Williams, R.S., 1990. The human amygdaloid complex: a cytologic and histochemical atlas using Nissl, myelin, acetylcholinesterase and nicotinamide adenine dinucleotide phosphate diaphorase staining. *Neuroscience* 36, 449–472.
- Sofroniew, M.V., Pearson, R.C., Eckenstein, F., Cuello, A.C., Powell, T.P., 1983. Retrograde changes in cholinergic neurons in the basal forebrain of the rat following cortical damage. *Brain Res.* 289, 370–374.
- Svendsen, C.N., Bird, E.D., 1985. Acetylcholinesterase staining of the human amygdala. *Neurosci. Lett.* 54, 313–318.
- Talairach, J., Tournoux, P., 1988. *Co-Planar Stereotaxic Atlas of the Human Brain*. Georg Thieme Verlag, Stuttgart.
- Thal, D.R., Rub, U., Orantes, M., Braak, H., 2002. Phases of A beta-deposition in the human brain and its relevance for the development of AD. *Neurology* 58, 1791–1800.
- Tiraboschi, P., Hansen, L.A., Alford, M., Masliah, E., Thal, L.J., Corey-Bloom, J., 2000. The decline in synapses and cholinergic activity is asynchronous in Alzheimer's disease. *Neurology* 55, 1278–1283.
- Verecken, T.H.L.G., 1993. *The Amygdaloid Complex in Alzheimer's Disease*. University Nijmegen, Nijmegen, NL.
- Wahlund, L.O., 1996. Magnetic resonance imaging and computed tomography in Alzheimer's disease. *Acta Neurol. Scand., Suppl.* 168, 50–53.
- Wevers, A., Schröder, H., 1999. Nicotinic acetylcholine receptors in Alzheimer's disease. *J. Alzheimer's Dis.* 1, 207–219.
- Wevers, A., Monteggia, L., Nowacki, S., Bloch, W., Schutz, U., Lindstrom, J., Pereira, E.F., Eisenberg, H., Giacobini, E., de Vos, R.A., Steur, E.N., Maelicke, A., Albuquerque, E.X., Schroder, H., 1999. Expression of nicotinic acetylcholine receptor subunits in the cerebral cortex in Alzheimer's disease: histotopographical correlation with amyloid plaques and hyperphosphorylated-tau protein. *Eur. J. Neurosci.* 11, 2551–2565.
- Whitehouse, P.J., Price, D.L., Struble, R.G., Clark, A.W., Coyle, J.T., DeLong, M.R., 1982. Alzheimer's disease and senile dementia: loss of neurons in the basal forebrain. *Science* 215, 1237–1239.
- Wienhard, K., Dahlbom, M., Eriksson, L., Michel, C., Bruckbauer, T., Pietrzyk, U., Heiss, W.D., 1994. The ECAT EXACT HR: performance of a new high resolution positron scanner. *J. Comput. Assist. Tomogr.* 18, 110–118.
- Zubieta, J.K., Koeppe, R.A., Frey, K.A., Kilbourn, M.R., Mangner, T.J., Foster, N.L., Kuhl, D.E., 2001. Assessment of muscarinic receptor concentrations in aging and Alzheimer disease with [<sup>11</sup>C]NMPB and PET. *Synapse* 39, 275–287.
- Zündorf, G., et al., 2002. PET functional parametric images of acetylcholine esterase activity without blood sampling. In: Senda, M., et al. (Eds.), *Brain Imaging Using PET*. Academic Press, San Diego, CA, pp. 41–46.